Rodríguez-Castellón, E.; Delgado-Muñoz, D.; Dejoz, A.; Vázquez, I.; Agouram, S.; Cecilia, JA.; Solsona, B.... (2020). Enhanced NiO Dispersion on a High Surface Area Pillared Heterostructure Covered by Niobium Leads to Optimal Behaviour in the Oxidative Dehydrogenation of Ethane. Chemistry - A European Journal. 26(42):9371-9381. https://doi.org/10.1002/chem.202000832

Enhanced NiO dispersion on a high surface pillared heterostructure covered by niobium leads to an optimal behaviour in the ODH of ethane

By

Enrique Rodríguez-Castellón[a]*, Daniel Delgado[b], Ana Dejoz[c], Isabel Vázquez[c], Said Agouram[d], Juan A. Cecilia[a], Benjamín Solsona[c], José M. López Nieto[b]*

[a] Departamento de Química Inorgánica, Facultad de Ciencias, Universidad de Málaga, 29071 Málaga, Spain. E-mail: castellon@uma.es

[b] Instituto de Tecnología Química, Universitat Politècnica de València-Consejo Superior de Investigaciones Científicas, Avenida de los Naranjos s/n, 46022 Valencia, Spain. E-mail: jmlopez@itq.upv.es

[c] Department of Chemical Engineering, Universitat de València, Av. Universitat s/n, 46100 Burjassot-Valencia, Spain. E-mail: Benjamin.Solsona@uv.es

[d] Department of Applied Physics and Electromagnetism, Universitat de València, C/Dr. Moliner 50, 46100 Burjassot, Valencia, Spain

*Enrique Rodríguez Castellón E-mail: castellon@uma.es, José Manuel López Nieto E-mail: jmlopez@itq.upv.es

Abstract

Nb-containing siliceous porous clay heterostructure (PCH) (Nb-content from 0 to 30 wt%), prepared from a bentonite, has been used as effective support in the preparation of supported NiO catalysts (with NiO loading from 15 to 80 wt%). Supports and NiO-containing catalysts have been characterized by several physicochemical techniques, and tested in the oxidative dehydrogenation of ethane. The characterization results on Nb-containing supports show the presence of well-anchored Nb^{5+} species, without the formation of Nb_2O_5 crystals. A high dispersion of nickel oxide (which presents a low crystallinity) has been observed when using the Nb-containing PCH supports. In addition, when NiO is supported on these Nb-containing porous clays, it displays a higher effectiveness in the ODH of ethane (ethylene selectivity of ca. 90 %) than NiO supported on the corresponding Nb-free siliceous PCH or on Nb_2O_5 (ethylene selectivity of ca. 30 and 60 %, respectively). Factors such as the NiO-Nb^{5+} interaction, NiO particle size and the properties of surface Ni^{n+} species have shown to be determining for the catalytic performance.

Keywords: ODH of ethane; supported nickel oxide; niobium oxide: heterostructure.

Introduction

The petrochemical industry presents two opposing forces in terms of the consumption pattern of its products. On the one hand, the decrease in the use of oil derivatives as fuels makes the future of petrochemicals look bright.[1] On the other hand, the future and present restrictions on the use of non-reusable and non-biodegradable plastics suggest a negative trend.[2,3]

Overall, the drastic reduction of oil as a fuel source opens a wide range of possibilities for oil to be used as raw material. Nowadays, ethylene is probably the most important feedstock of petrochemistry and it is very likely that its production will grow in the next years.[4] Unfortunately, the non-catalytic "steam cracking", which is the main route currently used for ethylene production, is one of the most energy-consuming processes in the chemical industry.[5,6] Among alternative processes, the catalytic oxidative dehydrogenation (ODH) of ethane, an exothermic reaction, stems as an interesting pathway that can sort out the main energy problem of steam cracking process.[7-9] For instance, in ODH an *in situ* re-oxidation of the surface of the catalyst takes place, what prevents its deactivation. Moreover, the fact that oxygen is fed together with ethane avoids coke formation, although carbon oxides are formed. In fact, the excessive formation of carbon oxides (COx), with the subsequent decrease in the selectivity to ethylene), is probably the main drawback reported up to date. Despite this, there exist two promising catalytic systems able to minimize undesired COx formation for the ODH of ethane: i) multicomponent MoVTeNb mixed oxides;[10-11] and ii) promoted or diluted NiO catalysts catalysts.[12-13]

NiO system can be considered a paradigmatic example of a host structure in which surface redox properties can be modulated to favour selective pathways in partial oxidation

reactions.[13-31] For example, unmodified NiO acts as a poor catalyst in the ODH of ethane, as it tends to transform ethane mainly into carbon dioxide, showing a low ability for ethylene formation. However, if doped/promoted with a suitable transition metal,[13-22] or diluted/supported on an appropriate metal oxide,[23-26] the formation of carbon dioxide can be minimized, thus reaching high selectivity to ethylene. Despite this, support/diluted- or dopant/promoter-induced effects, which provoke such a selectivity shift towards ethylene formation, are still unclear. For instance, a decrease in the electrical conductivity,[27,28] the reduction of NiO crystallite size,[29, 30] generation of defects,[25,30] , or the elimination of non-selective oxygen species [25,31] have been claimed as common effects that increase ethylene selectivity in the ODH of ethane, for both promoted and supported/diluted NiO catalysts.

Recently, we have compared the role of both Nb^{5+} or Ti^{4+} as promoters and their corresponding oxides as supports (i.e. Nb_2O_5 and TiO_2).[26] NiO catalysts, either promoted with Ti^{4+} or supported on TiO_2, display high selectivity to ethylene in the ODH of ethane (ca. 90 % selectivity). Conversely, a different trend is observed for Nb^{5+} or Nb_2O_5 in promoted or supported NiO-based catalysts. The incorporation of Nb^{5+} as dopant leads to highly selective catalysts (ethylene selectivity of ca. 90 %), as suggested previously.[12-18] On the other hand, supported NiO/Nb_2O_5 catalysts do not exceed a 60-65 % selectivity to ethylene,[31] due to an ineffective active phase-support interaction.

Accordingly, in the present work we have evaluated the possibility to prepare a supported NiO catalyst, with the presence of dispersed niobium species on the support, in order to selectively transform ethane into ethylene by ODH. For this purpose, a bentonite has been modified to obtain a structure with higher surface area, denoted as porous clay heterostructure (PCH). This porous material was used as support to disperse Nb_2O_5 (Nb-content from 0 to 30 wt.% of Nb_2O_5) and NiO (with NiO loading from 15 to 80 wt.%).

This catalytic system was evaluated in the ODH of ethane. The results are discussed in terms of the ability of surface Nb^{5+} species present on PCH to modify the physicochemical characteristics of NiO.

Results

Characterization of supports

Physicochemical characteristics of supports (i.e. Nb-free and Nb-containing siliceous porous clay heterostructure, with Nb-content from 0 to 30 wt.% Nb_2O_5) are summarized in Table 1.

In a first approximation, supports were analysed by powder X-ray diffraction (XRD), and their corresponding XRD patterns are displayed in **Figure S1** (Supporting information). The first important feature observed in XRD profiles is that Bragg lines corresponding to crystalline Nb_2O_5 are not observed in any of Nb-containing supports. Considering that pseudohexagonal Nb_2O_5 phase is already formed at 500 ºC,[32] its absence could indicate that well-anchored NbO_x species are formed on PCH surface, as it will be discussed below.

To shed some light on the nature of these niobium species, supports were studied by means of diffuse reflectance UV-VIS spectroscopy. **Figure 1** shows diffuse reflectance UV-VIS spectra of Nb_2O_5 and Nb-PCH supports. Interestingly, Nb-free PCH support shows negligible absorption (**Figure 1**, *spectra a*). According to this, the sharp absorption signals found in all Nb-containing supports (**Figure 1**, *spectra b* to *e*) must arise from electronic transitions due to the presence of Nb species on PCH. In this sense, the absorption edge is shifted to higher wavenumbers when the amount of Nb on the support increases. We have estimated the band-gap energies by applying Tauc´s method (E_{gap})

(see **Table 1**, and insets in **Figure 1**).[33, 34] It can be noted that E_{gap} values differ for Nb-containing PCH supports (i.e. supports B, C and D with E_{gap} between 4.3-4.4 eV) and bulk Nb_2O_5 (E_{gap}= 3.4 eV), underlining the different nature of Nb species in both materials.

Figure 1. Diffuse reflectance UV-VIS spectra and their corresponding Tauc plots of supports. a) Support A (PCH); b) Support B (5 wt.% Nb_2O_5 on PCH); c) Support C (15 wt.% Nb_2O_5 on PCH); d) Support D (30 wt.% Nb_2O_5 on PCH); e) Nb_2O_5.

The position of the absorption edge (and subsequently E_{gap} values) is directly dependent on the electronic structure of the absorbing species, which is linked to their specific chemical environment and structural features.[35] According to the structural and spectroscopic analysis of supports, this shift to higher energy band-gaps in Nb-containing PCH materials can be ascribed to the presence of well-anchored Nb^{5+} sites, rather than to the formation of Nb_2O_5.[36] This improved dispersion of Nb^{5+} would be responsible for the hindered sinterization towards Nb_2O_5. These findings are in agreement with the characterization results reported by Kondo and coworkers,[36] who found a similar effect on NbO_x- SBA-15 system, in which the authors were able to control the growth of mono- bi- and tri-layered niobium oxide on the surface of the mesoporous silica, without Nb_2O_5 formation. The analyses of the supports by TEM and EDX show the homogeneous distribution of Nb on the porous support (Fig. S2, Supporting Information).

The surface chemical nature of these Nb species was analysed by XPS. **Figure 2** presents Nb 3*d* core-level XPS spectra of Nb-containing supports, showing Nb $3d_{5/2}$ lines in the range 207-208 eV, typical of Nb^{5+} species.[37, 38]

Figure 2. Nb 3d core-level XPS spectra of Nb-containing supports, i.e. supports B, C and D. For comparison the spectrum of pure Nb_2O_5 has been also included.

It can be observed that Nb $3d_{5/2}$ peak shifts to higher binding energies for Nb-containing PCH supports (B.E. = 207.9 eV), with respect to bulk Nb_2O_5 (B.E. = 207.0 eV) (**Figure 2**). This effect goes in line with our previous statements, by which an effective interaction between Nb^{5+} and PCH support gives rise to dispersed Nb^{5+} sites, displaying a different chemical nature than those Nb entities found in Nb_2O_5.[36]

Characterization of supported NiO catalysts

Taking into consideration the different nature of Nb species detected on the supports, we have carried out the synthesis of a series of supported NiO catalysts. The physicochemical features of supported catalysts are summarized in **Table 2**.

Figure 3 displays powder XRD patterns of supported NiO materials. All the catalysts present the characteristic diffraction lines of NiO (Fm3m, JCPDS: 04-0835). Depending on the type of support and on NiO-loading, changes in the diffraction profiles are observed, especially in line-broadening of NiO peaks. FWHM of Bragg peaks is directly related with average crystallite size of NiO, which has been reported to be one of the key factors to increase the activity and selectivity of these materials in the ODH of ethane.[29, 39]

For instance, increasing NiO-loading on Support C (15 wt.% Nb_2O_5 on PCH) decreases NiO diffraction line width, indicating an increase in NiO particle size (**Figure 3a** and **Table 2**). On the other hand, when comparing different supports at a fixed NiO loading

(50 wt.% NiO), width of NiO Bragg peaks increases with Nb content on PCH (from 0 to 15 wt.% Nb_2O_5) (**Figure 3b**, 50Ni/A, 50Ni/B and 50Ni/C, respectively). This indicates a decrease of NiO crystallite size when relatively low amounts of Nb are incorporated on PCH (**Table 3**), suggesting an effective interaction between the support and NiO. However, if higher Nb-loadings are incorporated (50Ni/D, 30 wt.% Nb_2O_5 on PCH), the average NiO particle size increases drastically, as it can be inferred from the narrow NiO peaks observed for 50Ni/D catalyst **(Figure 3b** and **Table 2**). In addition, no Bragg peaks corresponding to Nb_2O_5 phases were detected in any catalyst.

Figure 3. XRD patterns of supported NiO catalysts. Characteristics of catalysts in Table 1. For comparison the XRD patterns of pure NiO and support C has been also included.

To corroborate the effect of supports on the morphology and distribution of supported nickel oxide particles, samples with a 50 wt.% NiO-loading were further analysed by TEM and EDX (**Figure 4**). When NiO is supported on unmodified PCH siliceous support (Support A), nickel oxide particles (detected by selected-area electron diffraction) with size in the range 5-30 nm are observed (**Figure 4**, 50Ni/A). On the other hand, if the active phase is deposited on PCH with low and intermediate Nb contents (5 and 15 wt.% Nb_2O_5; Support B and C, respectively), NiO particle size decreases down to 5-20 nm for 50Ni/B and 3-10 nm for 50Ni/C catalyst (**Figure 4**). In all cases, EDX analyses show a good dispersion of NiO along the support in these three catalysts. In contrast, when the amount of Nb deposited on PCH is increased up to 30 wt.% Nb_2O_5 (Support D), the particle size of supported NiO particles increases, falling in the range 20-40 nm (**Figure 4**, 50Ni/D). This confirms that, low/intermediate Nb-loadings on PCH favour a smaller particle size of NiO.

Figure 4. TEM images and their corresponding EDX maps of supported NiO catalysts with 50 wt% of NiO: 50NiO/A; 50NiO/B; 50 NiO/C; and 50NiO/D.

Supported catalysts (with a 50 wt.% NiO) were also characterized by Raman spectroscopy (**Figure 5**). The samples were irradiated with an UV-laser (325 nm), since conventional Raman experiments conducted using a 514 nm radiation source resulted in extremely noisy spectra, masked by Raman fluorescence phenomena. Interestingly, UV-Raman spectroscopy has been reported to be more sensitive to the surface region of solid materials,[40, 41] what makes it more suitable to study solid catalysts. All the spectra display four Raman bands that can be unambiguously assigned to NiO. These signals correspond to one-phonon (1P) TO (transverse optical) and LO (longitudinal optical) modes (at ~570 cm^{-1}), two-phonon (2P) 2TO modes (at~730 cm^{-1}), TO + LO (at ~906 cm^{-1}) and 2LO (at ~1090 cm^{-1}) modes (**Figure 5**).[42, 43]

Figure 5. UV-Raman spectra of UV-Raman spectra of supported NiO catalysts with 50 wt% of NiO: 50NiO/A; 50NiO/B; 50 NiO/C; and 50NiO/D.

The disorder-induced 1P (LO) band at ~570 cm^{-1} presents low intensity when NiO is supported on PCH (**Figure 5**, 50Ni/A). Interestingly, the relative intensity of 1P (LO) band increases for 50NiO/B and 50Ni/C, i.e. at intermediate Nb-loadings on PCH (5 and 15 wt.% Nb_2O_5) (**Figure 5**). Conversely, at higher Nb contents on the support (30 30 wt.% Nb_2O_5, Support D), the intensity of 2P modes of NiO increases notably (**Figure 5**, 50Ni/D). These spectral features can be explained in terms of NiO particle size. This way, the relative intensity of 1P band will increase concomitantly with: i) the decrease of NiO

particle size and; ii) the presence of defects. It is worth mentioning that the most selective catalysts in the ODH of ethane (as it will be discussed later) show the highest relative intensity of LO (1P) Raman band. This could indicate a relationship between selectivity to ethylene in the ODH of ethane and particle size and/or concentration of defects, as it was previously suggested in literature.[30]

The effect of NiO-loading and type of support on the reducibility of supported NiO catalysts was studied by means of temperature-programmed reduction (TPR-H_2) (**Figure 6**). H_2 up-takes measured during the experiments correspond to the reduction of NiO theoretical amounts added in each catalyst (**Table 2**).

Figure 6a displays TPR-H_2 profiles of NiO supported on PCH with a 15 wt.% Nb_2O_5 (Support C). Unmodified NiO presents its main reduction peak at ca. 296ºC, showing a shoulder at 315ºC, which is the typical reduction profile of bulk NiO.[29, 30] It can be seen that increasing NiO-loading on Support C, leads to a shift of the main reduction peak towards lower temperatures, indicating an increased reducibility (**Figure 6a**).

If we compare TPR-H_2 profiles at a fixed 50 wt.% NiO-loading, it can be found that, regardless of the support used, the catalysts present a lower reducibility than bulk NiO, displaying their maximum H_2 consumption in the range 350-380 ºC (**Figure 6b**). Despite this, 50Ni/C catalyst shows a slightly lower reducibility than the rest of materials (reduction peak centred at 375 ºC), which in addition presents the smallest NiO particle size (**Figure 6b**, 50Ni/C).

Figure 6. TPR-H_2 profiles of: a) Supported NiO catalysts, using Support C (i.e. with 15 wt.% Nb_2O_5 on PCH); b) supported NiO catalysts with 50 wt% of NiO.

To evaluate the effect of Nb-containing supports on the nature of surface Ni species, catalysts with a 50 wt.% NiO were studied by XPS. **Figure 7** shows Ni 2*p* core-level spectra of 50 wt.% NiO supported catalysts, using supports with increasing Nb-loadings (0, 5, 15, 30 wt.% Nb_2O_5 on PCH, Supports A, B, C and D respectively). For comparison, Ni $2p_{3/2}$ core-level spectra of NiO/Nb_2O_5 and unsupported NiO are shown in **Figure S3** (Supporting information). All the spectra display the typical features of Ni 2*p* core level: i) a main peak at ca. 854-855 eV, assigned to Ni^{2+} surface species, and; ii) two satellite structures (Sat I and Sat II) (**Figure 7**). Sat I, located at ca. 1.5 eV over the main peak, is attributed to different types of surface defects such as, Ni^{2+} vacancies,[44, 45], Ni^{2+}-OH sites [46] or the presence of Ni^{3+} species.[47] Variations in the relative intensity of this peak have, in some cases, been ascribed to changes in NiO particle size.[45] On the other hand, the appearance of Sat II structure at ca. 7 eV over the main peak, is assigned to metal-ligand charge transfer.[44, 46, 48] Although XPS spectral features are still under debate, the spectra show that, when NiO is supported on Nb-containing supports, the relative intensity of Sat I peak increases, suggesting a higher active-phase support interaction (**Figure 7**).

Figure 7. Ni 2*p* core-level spectra of supported NiO catalysts with 50 wt% of NiO: a) 50NiO/A; b) 50NiO/B; c) 50 NiO/C; and d) 50NiO/D.

Since Nb-containing siliceous porous clays heterostructures present an effective interaction with the active phase (i.e. they are able to modify structural and chemical characteristics of NiO), we decided to study the chemical nature of surface Nb species in 50 wt.% NiO supported catalysts by XPS. **Figure 8** presents Nb 3*d* core-level XPS spectra of NiO supported catalysts. The spectra show differences depending on Nb content in the support. At relatively low Nb concentration on the support (5 and 15 % Nb), the samples

display a single Nb $3d_{5/2}$ XPS peak centred at 207.9 eV, which can be assigned to anchored Nb^{5+} species (**Figure 8**, *spectra a* and *b*, respectively).[36] When increasing the amount of Nb incorporated on siliceous porous clays heterostructures, a new peak at lower binding energies (ca. 206.5 eV) appears in the spectra (**Figure 8**, *spectra c*), which can be assigned to Nb^{5+} in Nb_2O_5.[37, 38]

Figure 8. Nb 3*d* core-level spectra of Nb-containing supported NiO catalysts with 50 wt% of NiO: a) 50NiO/B; b) 50 NiO/C; and c) 50NiO/D.

On the other hand, diffuse reflectance UV-VIS spectra for the series of supported NiO catalysts with a 50 wt.% NiO loading show similar features than those observed on the Nb-containing supports: i) a red shift in the absorption edge when Nb-content in the support increases (**Figure S4**, Supporting information); and ii) an increase in the E_{gap} value when NiO is supported on Nb-containing PCH (**Table 1** and **Figure S5** in Supporting information).

In summary, spectroscopic analysis of supports and catalysts, show that two types of Nb species can exist in the catalysts: i) well-dispersed Nb^{5+} species at low Nb-loadings on PCH, which are able to substantially modify NiO (particle size, number of defects, etc.) and, ii) Nb^{5+} sites similar to those observed in Nb_2O_5 (appearing at high Nb-loadings on the support). The use of Nb-containing PCH as supports for NiO improves the dispersion of NiO in comparison with unmodified PCH and Nb_2O_5.

Catalytic results in the ODH of ethane

According to the changes in the chemical nature of NiO induced by the different supports (particle size, reducibility, concentration of defects…), NiO-containing catalysts were tested as catalysts for the oxidative dehydrogenation (ODH) of ethane (**Table 3**). During the catalytic tests, the only reaction products observed were ethylene and CO_2. Traces of CO cannot be discarded, although, if present, the selectivity should be lower than 1%.

Figure 9a compares the catalytic activity (in g_{C2} kg_{cat}^{-1} h^{-1}) of xNiO/C series with different NiO contents. It can be observed that catalytic activity increases with the NiO-loading until 50 wt.% NiO (**Figure 9a**). For higher NiO loadings the catalytic activity is kept rather stable. However, if the activity per gram of NiO is considered, there exists a clear maximum at 50 wt.% NiO (**Table 3**).

We have also compared the activity of 50 wt.% NiO catalysts supported on PCH with increasing Nb-loading (Supports A-D with 0 to 30 wt.% Nb_2O_5). The catalytic results are shown in **Figure 9b**. In this case, the activity increases with the Nb content until reaching a maximum at 15 wt.% Nb_2O_5 (50Ni/C) (**Table 3**). Further increasing Nb-loading in the support (i.e. Support D, with 30 wt.% Nb_2O_5) leads to a decrease in the catalytic activity.

Figure 9. Influence of NiO loading (for catalysts of xNiO/C series) (**a**) and influence of Nb-loading on support (for catalysts with 50wt% of NiO) (**b**) on catalytic activity (in g_{C2} kg_{cat}^{-1} h^{-1}) during the ODH of ethane over supported NiO catalysts. Reaction conditions: $C_2/O_2/He$ = 3/1/26 molar ratio, T = 450ºC and W/F = 4 g_{cat} h mol_{C2}^{-1}.

Provided that the differences in activity are not of orders of magnitude, the selectivity to ethylene is a more important factor to consider in order to determine the efficiency of this series of catalysts. Accordingly, the catalytic performance of supported NiO catalysts has

been studied by using different contact times (i.e. varying catalyst weight or the total flow) and fixing reaction temperature and C_2/O_2/He ratio. This way, we can compare the selectivity to ethylene in the ODH of ethane at a given conversion.

Figure 10a displays the variation of ethylene selectivity with NiO content for xNi/C series at isoconversion conditions (i.e. ethane conversion of 10% at 450 ºC). It can be noted that the selectivity to the olefin increases concomitantly with NiO-loading, reaching the maximum at 50 wt.% NiO (catalyst 50Ni/C; $S_{ethylene}$= 87 %). Higher NiO loadings led to a decrease in the selectivity to ethylene.

Figure 10. a) Variation of the selectivity to ethylene as a function of NiO-loading on Support C (15 wt.% Nb_2O_5 on PCH. b) Variation of the selectivity to ethylene as a function of ethane conversion for supported 50 wt.% NiO catalysts. Reaction conditions as in Fig. 9.

We have also analysed the catalytic behaviour 50 wt.% NiO catalysts supported over PCHs materials with increasing Nb-loading (Supports A-D). **Figure 10b** shows the variation of the selectivity to ethylene in the ODH of ethane as a function of ethane conversion for 50 wt.% NiO catalysts at 450 ºC. It is worth mentioning that, regardless of the nature of the catalysts, the selectivity to ethylene barely varies with ethane conversion under the reaction condition applied in the study. This means that, even for the less selective materials, the deep oxidation of the olefin to carbon oxides does not take place, i.e. carbon oxides are essentially formed directly from ethane.[49]

Despite this, variations in the selectivity to ethylene in the ODH of ethane are observed depending on the nature of the support (**Figure 10b**). When NiO is supported on

unmodified PCH, a low selectivity to ethylene (of ca. 38 %) is achieved (**Figure 10b**, 50Ni/A). This selectivity lies in the range of that reached on bulk NiO (ca. 33 %) (**Table 3**), indicating that the unmodified PCH support is not able to provide an effective active-phase support interaction. On the other hand, when NiO on a PCH support with 5 wt.% Nb_2O_5 (Support B), the selectivity to the olefin drastically increases, up to 67 % (**Figure 10b**, 50Ni/B), which is slightly higher than the one achieved on the Nb_2O_5-supported catalyst (ca. 59 %) (**Table 3**). By increasing the amount of Nb deposited on PCH up to 15 wt.% Nb_2O_5 (Support C), the selectivity to ethylene further increases, up to ca. 87 %, which is in the range of the best NiO-based catalysts reported in the literature (for instance, Nb-doped NiO catalysts)[13] (**Figure 10b**, 50Ni/C). However, if higher amounts of Nb are deposited on PCH support (30 wt.% Nb_2O_5, Support D), selectivity to ethylene drops down to ca. 64 % (**Figure 10b**, 50Ni/D).

Then, it seems that the impregnation of an appropriate amount of Nb on a bentonite-derived PCH material (and the subsequent addition of NiO) leads to a drastic improvement in the selectivity to ethylene in the ODH of ethane, from ca. 38% (50Ni/A catalyst, i.e. when using a Nb-free support) to ca. 87% (50Ni/C catalyst). Moreover, the use of a matrix such as the pillared clay to deposit niobium is necessary to obtain efficient catalysts. In this sense, the use of the Nb-modified porous clay support leads to an improvement in the selectivity to ethylene from ca. 60% (50Ni/Nb_2O_5) to ca. 87% (50Ni/C). Therefore, to achieve optimal results in the ODH of ethane, the presence of a high surface area material on which niobium oxide can be dispersed is necessary. Thereby, the absence of either niobium or PCH gives rise to an ineffective NiO-support interaction, leading to low ethylene selectivity (ca. 30-60 %).

We want to mention that these catalytic results have been obtained using C_2/O_2 ratio of 3. However, the use of a feed richer in oxygen leads to a slight drop in the selectivity to

ethylene. Then, over 50Ni/C catalyst, using W/F = 2 g_{cat} h mol_{C2}^{-1} and a C_2/O_2 ratio of 1 (C_2/O_2/He = 1/1/8 molar ratio), the ethane conversion is 10.7% and the selectivity to ethylene is 82.3%.

Discussion

In this study we have shown that by dispersing niobium on a high surface area porous clay heterostructure (PCH) material, a suitable support for NiO can be synthesized. NiO catalysts supported on Nb-containing PCH display an enhanced catalytic performance in the ODH of ethane, compared to formulations in the absence of PCH (NiO/Nb_2O_5)[31] or Nb-free PCH (NiO/PCH, this work). Interestingly, as it takes place in Nb-promoted NiO catalysts,[13-16] in our supported catalysts the Nb-loading should be controlled to optimize the catalytic results. Then, an appropriate amount of niobium must be deposited on the surface of the PCH matrix. Then, the optimal Nb-loading corresponds to 15 wt.% Nb_2O_5 (Support C). Lower or higher Nb-loadings on PCH support (5 or 30 wt.% Nb_2O_5, respectively) lead to supported NiO catalysts presenting a lower ethylene formation in the ODH of ethane. Despite this, NiO/Nb-PCH materials display an improved catalytic behaviour (in terms of ethylene selectivity), with respect to NiO supported on PCH (sample 50NiO/A) or supported on Nb_2O_5 (sample $50Ni/Nb_2O_5$).

For bulk NiO catalysts, NiO crystallite size has been demonstrated to play an important role in olefin formation in the ODH of ethane.[29, 30] By modifying the synthesis procedure (for instance, adding organic additives, [39] or transition metal promoters[29]), it is possible to decrease NiO average crystallite size, what generally leads to higher ethylene selectivity. In the same way, the addition of low/intermediate amounts niobium on PCH support (0-15 wt.% Nb_2O_5, Supports B and C) favours a lower NiO crystallite size, an

improved NiO dispersion and a higher selectivity to ethylene. On the contrary, higher Nb-loadings on PCH (30 wt.% Nb_2O_5, Support D) give rise to bigger NiO particles and a decrease in ethylene selectivity.

Figure S6A shows the variation of ethylene selectivity (measured at isoconversion conditions, 10 % ethane conversion) as a function of NiO crystallite size for all synthesized materials. For Nb-containing catalysts, the selectivity follows a quite defined trend, in a way that the lower the NiO crystallite size, the higher the selectivity to ethylene. However, selectivity levels for Nb-free catalysts are far below the levels that would correspond to the same NiO crystallite size in Nb-containing catalysts. These observations suggest that other factors (apart from the particle size) have to be taken into consideration to explain the catalytic performance of these materials (such as reducibility, nature of surface Ni sites or NiO-support interaction),

The reducibility of nickel oxide species can have some influence on the selectivity to ethylene achieved.[13-29, 31] Since reducibility is not a parameter easy to be quantified, we have selected the temperature for the maxima of the main TPR peak as a reference value. This way, the higher the reduction temperature, the lower the reducibility of Ni^{n+} sites on the catalyst. Figure S6B (supporting information) shows the variation of the selectivity to ethylene measured at isoconversion conditions (10 % ethane conversion) as a function of the maximum H_2-consumption temperature in H_2-TPR profiles for each NiO-based catalyst. It can be seen that the most selective catalysts are those with the lowest reducibility. This suggests that highly reducible nickel oxide species are prone to activate ethane in a non-selective way, thus directing the reaction towards total oxidation, rather than to oxidative dehydrogenation.[26]

Characterization results of supports and supported NiO catalysts indicate that we can have two different types of Nb sites with different chemical nature: i) Nb^{5+} site that are well anchored to PCH support and, ii) Nb^{5+} species similar to those found in Nb_2O_5. Depending on the type of Nb on the support, variations in NiO-support interaction will take place, thus giving rise to different NiO particles showing a different selectivity to ethylene in the ODH of ethane.

Interestingly, the relative intensity of Sat I peak in the XPS spectra slightly increases with respect to the main peak when Nb is incorporated in the PCH support, concomitantly with the increase in the selectivity to ethylene in the ODH of ethane (**Figure 7**). This fact suggests that the support does not exclusively modulates NiO particle size, but also modifies the concentration of defects in the active phase, like Ni^{3+}, Ni^{2+} vacancies or Ni^{2+}-OH surface sites, which can play a key role in the catalytic behaviour. For example, the presence of Ni^{3+} species has been linked with a higher concentration of electrophilic oxygen species, responsible for total oxidation.[50]

On the other hand, Ni 2*p* XPS spectra of the less selective catalysts, i.e. 50NiO/A (**Figure 7**, *spectra a*), NiO/Nb_2O_5 (**Figure S2**, spectra a; *Supporting information*) and unsupported NiO (**Figure S2**, spectra b; *Supporting information*), display high similarities, particularly a low Sat I/Main peak ratio. Accordingly, it seems that these supports are not able to interact efficiently with NiO, leading to similar Ni^{n+} surface sites and, subsequently, to a low selectivity to ethylene in the ODH of ethane (ca. 30-60 %).

We must underline that supports used (unmodified PCH or Nb-containing PCH) show a negligible conversion of ethane under the reaction conditions used in this study. Therefore, the reactivity is completely determined by the catalytic potential of the nickel oxide. In the case of Nb-free 50Ni/A catalyst, NiO-support interactions will be dominated

by NiO-silica contact, which is not able to modify the chemical nature of NiO.[30] Thus, a low selectivity to ethylene in the ODH of ethane is achieved (ca. 30 %, similar to that observed for unsupported NiO). In the same line, 50NiO/Nb_2O_5 does not interacts efficiently with NiO, leading to low NiO dispersion and large NiO particles similar to those in non-selective NiO.[31] On the contrary, when NiO is supported on Nb containing PCH materials, a drastic increase in the selectivity to ethylene is observed (up to 87 % for 50Ni/C catalyst). Unlike in the case of Nb_2O_5, Nb species present on these supports are able to interact in an efficient way with NiO. The efficiency of this active phase-support interaction will depend fundamentally on the amount of Nb loaded in on the porous clay heterostructure.

At low Nb-loadings (5 wt.% Nb_2O_5 on PCH, 50Ni/B catalyst), at which the optimum Nb-coverage is not achieved, the support presents two main regions susceptible to interact with NiO: i) dispersed Nb^{5+} surface sites and; ii) uncovered PCH silica-rich zones. The interaction between well-anchored Nb^{5+} sites leads to selective sites in the ODH of ethane, whereas interaction between NiO and SiO_2 zones on PCH gives rise to unselective sites (similar to those found in unsupported NiO). Then, for 50Ni/B sample (5 wt.% Nb_2O_5 on PCH), higher selectivity to ethylene is observed (ca. 67 %), in comparison with PCH-supported catalysts (50Ni/A, presenting a selectivity to ethylene of 38 %). Consequently, it is possible to optimize the catalytic performance of this system by incorporating increasing amounts of Nb on the support. This way, when using a 15 wt.% Nb PCH support for NiO (50Ni/C catalyst) we are favouring the desired Nb^{5+}-NiO interaction, minimizing the exposure silica zones on the support, thus achieving a high selectivity to ethylene in the ODH of ethane (ca. 87 %). However, if relatively high amounts of Nb are deposited on PCH support (30 wt.% Nb_2O_5 on PCH, 50Ni/D catalyst),

the segregation of bulk Nb_2O_5 can take place, leading to bigger NiO particles, a lower dispersion of the active phase, and a decrease of the selectivity to the olefin (ca. 64 %).

One of the main problems of the Nb-promoted NiO catalysts is their lack of stability with the time on stream. This instability has been related to the formation of the less active $NiNb_2O_6$ phase[13, 16] and the reduction of the amount of active oxygen in NiO[16-21] and to a decrease in the surface area. [16, 51] We have wanted to check if our supported catalysts also present that instable behaviour. After 8 h on line, 50Ni/C catalyst presented a slight decrease of the ethane conversion (Figure S7, Supporting information) together with a slight increase in the ethylene selectivity. A further study for longer times would be required to determine the industrial applicability of these materials.

Conclusions

In summary, it has been proven that it is possible to prepare efficient supported NiO catalysts for the ODH of ethane, by using Nb-modified porous clay heterostructures (Nb-PCH) as supports. NiO catalysts supported on Nb-PCH materials present an enhanced selectivity to ethylene (up to ca. 90%) with respect to PCH- and Nb_2O_5-supported nickel oxide catalysts, which shows a selectivity to ethylene of ca. 30 and 60%, respectively).

While Nb_2O_5 and unmodified PCH do not modify the chemical nature of NiO, Nb-containing PCH supports are able to: i) decrease NiO particle size; ii) induce changes on Ni^{n+} surface sites and; iii) decrease the reducibility of Ni^{n+} species. According to catalytic results, the key factor to achieve a high selectivity to ethylene in the ODH of ethane is to control NiO-support interaction. This can be achieved by controlling Nb-loading on the support. Thus, Nb-loadings of 15wt.% Nb_2O_5 deposited on PCH minimize non-selective silica zones exposed on the surface, thus leading to an ethylene selectivity values in the range of the best catalysts reported in the literature.

Characterization of Nb-containing supports and catalysts demonstrate that Nb^{5+} species on PCH present a different chemical nature than that observed in Nb_2O_5. Specifically, XRD, XPS and UV-VIS results suggest that Nb^{5+} species are dispersed and well-anchored on PCH surface. These species are able to interact efficiently with NiO, giving rise to an excellent catalytic performance in the ODH of ethane, which is not the case of Nb^{5+} sites in Nb_2O_5.

Experimental Section

Preparation of Supports and catalysts

A bentonite from "Sierra de Níjar" (Spain) supplied by Minas de Gador S. A. was used as the raw material. The bentonite presents a high proportion of montmorillonite as reported in previous studies.[26] Prior to the synthesis, montmorillonite phase was collected by sedimentation and treated with a solution of NaCl for 1 day to obtain the homoionic montmorillonite (Na-mont). More details of the preparation are shown elsewhere.[26] Si-pillars were then dispersed in an n-propanol solution with a ratio Si/n-propanol = 1 and added to the previous suspension, and stirring for 3 days. The source of silicon used was tetraethyl orthosilicate (Aldrich). Then, the gel was filtered and washed with water and ethanol and dried at 60 °C in air for 12 h. Finally the surfactant was removed by calcination in air at 550 °C for 6 h. Thus, the sample with Si-pillars, a siliceous porous clay heterostructure (PCH), was named as support A.

Nb-containing siliceous porous clay heterostructure were prepared by adding solutions of niobium oxalate monooxalate adduct, i.e. $C_{10}H_5NbO_{20}$ (ABCR), to the PCH support. After evaporation under vigorous stirring the paste obtained was dried at 120ºC overnight

and then calcined at 500ºC for 2h in static air. Thus, Nb-containing supports have been named as B, C or D for samples with a Nb content of 5, 15, or 30 wt.%, respectively. The characteristics of supports are shown in Table 1.

Supported NiO catalysts were synthesized as follows: an ethanolic solution of nickel(II) nitrate $Ni(NO_3)_2 \cdot 6H_2O$ and oxalic acid (both from Sigma-Aldrich) was prepared (oxalic acid/Ni molar ratio of 3). To this mixture a porous clay heterostructure (PCH) derived from bentonite with or without niobium (samples A, B, C or D) was added. After evaporation in a hot plate stirrer and drying at 120ºC overnight, the catalysts were calcined at 500ºC for 2h in static air. The catalysts have been named as xNi/support (support= A, B, C or D), x being the NiO wt% content. For example, the catalyst 50Ni/C contains 50 wt.% NiO, the support consisting of 15 wt.% Nb_2O_5 deposited on BG (sample C).

Diluted NiO/Nb_2O_5 catalysts were synthesized as follows: an ethanolic solution of nickel nitrate $Ni(NO_3)_2 \cdot 6H_2O$ and oxalic acid (both from Sigma-Aldrich) was prepared (oxalic acid/Ni molar ratio of 3). To this mixture niobium oxide (hydrothermally synthesized, see reference[31]; S_{BET} = 70 m^2 g^{-1}) was added. Then the mixture was vigorously stirred at 60ºC until a paste was achieved. This material was introduced in a furnace and kept at 120 ºC overnight and then was heat-treated in static air for 2 h at 500 ºC. The catalysts have been named as $50NiO/Nb_2O_5$ (i.e. 50 wt% content of NiO). The characteristics of catalysts are shown in Table 2.

Characterization

Powder X-ray diffraction patterns were recorded in a powder diffractometer model D8 Avance A25 Bruker brand with a CuKα source operated at 40 kV and 40 mA.

Transmission electron microscopy (TEM) images, selected-area electron diffraction (SAED) patterns and Energy-dispersive X-ray spectroscopy (EDX) maps were collected in a field-emission gun TECNAI G2 F20 S-TWIN electron microscope, operating at 200 kV. Samples were sonicated in ethanol and deposited on a copper grid prior to analysis.

N_2-adsorption isotherms were recorded in a Micromeritics ASAP 2000 device. The materials were degassed in vacuum at 300 ºC prior to N_2 adsorption. Surface areas were estimated by the Brunauer-Emmet-Teller (BET) method.

Raman spectroscopy was carried out in an inVia Renishaw spectrometer equipped with an Olympus microscope, at an exciting wavelength of 325 nm.

Temperature-programmed reduction in H_2 (TPR-H_2) was carried out in a Micromeritics Autochem 2190 instrument, equipped with a thermal conductivity detector (TCD). Samples were heated up to 800 ºC (heating rate of 10 ºC min^{-1}) using a reductive mixture of 10 % H_2 in Ar, at a total flow of 50 mL min^{-1}.

XPS measurements were carried on a Physical Electronics spectrometer (PHI Versa Probe II Scanning XPS Microprobe with monochromatic X-ray Al Kα radiation (100 μm, 100 W, 20 kV, 1486.6 eV) and a dual-beam charge neutralizer. The spectrometer was calibrated with Au $4f_{7/2}$, Ag $3d_{5/2}$ and Cu $2p_{3/2}$ photoelectron lines at 84.0, 368.2 and 932.7 eV, respectively. The Au $4f_{7/2}$ line was recorded with 0.73 eV FWHM at a binding energy (BE) of 84.0 eV, under a constant pass energy mode at 23.5 eV condition. XPS spectra were analysed using PHI SmartSoft software and processed using MultiPak 9.3 package. The binding energy values for the measured spectra were referenced to C 1*s* signal of adventitious carbon at 284.8 eV. Recorded spectra were fitted using Gauss–Lorentz curves. Atomic concentration percentages of the constituent elements of the surfaces were

determined taking into account the corresponding area sensitivity factor for the different measured spectral regions.

Diffuse-reflectance UV-VIS spectra were recorded in a Cary 5000 spectrophotometer, in the 200-800 nm wavelength range.

Catalytic tests for ethane ODH

The catalytic experiments were carried out under steady state conditions using a fixed-bed quartz tubular reactor working at atmospheric pressure.[26] The flow rate (25–100 ml min^{-1}) and the amount of catalyst (0.1–0.3 g, 0.3–0.5 mm particle size) were varied in order to achieve different ethane conversion levels at a given reaction temperature. The feed consisted of a mixture of ethane/oxygen/helium with molar ratio of 3/1/26. Experiments were carried out in the 350-450 ºC temperature range. Reactants and reaction products were analysed by on-line gas chromatography, using two packed columns: [26] (i) Porapak Q (3 m); and ii) molecular sieve 5 Å (2.5 m).

Acknowledgements

The authors would like to acknowledge the DGICYT in Spain (CRTl2018-099668-B-C21, RTl2018-099668-B-C22 and MAT2017-84118-C2-1-R projects). Authors from ITQ also thank Project SEV-2016-0683 for supporting this research. D.D. thanks MINECO and Severo Ochoa Excellence Program for his fellowship (SVP-2014-068669).

References

[1] L. Nichols, Industry Perspectives: Global petrochemical sector to see robust growth to 2020, *Hydrocarbon Processing* **2017. March.**

[2] L. Hermabessiere, A. DehautaIk, P. Pont, C. Lacroix, R. Jezequel, P. Soudant, G. Duflos, *Chemosphere* **2017**, 182, 781-793.

[3] L. Jia, S. Evans, S. van der Linden, *Nature* **2019**, 4582.

[4] M. Ghanta, D. Fahey, B. Subramaniam, *Appl. Petrochem. Res.* **2014**, 4, 167–179.

[5] T. Ren, M.K. Patel, K. Blok, *Energy* **2006**, 31, 425–451.

[6] T. Ren, M.K. Patel, K. Blok, *Energy* **2008**, 33, 817–833.

[7] F. Cavani, N. Ballarini, A. Cericola, *Cat. Today* **2007**, 127, 113–131.

[8] J.M. López Nieto and B. Solsona in *Metal Oxides in Heterogeneous Catalysis* (Eds. J.C. Vedrine), Elsevier, **2018**, pp. 211-286

[9] Ch. A Gärtner, A. C. van Veen, J.A. Lercher, *ChemCatChem* **2013**, 5, 3196-3217.

[10] J.M. López Nieto, P. Botella, M.I. Vazquez, A. Dejoz, *Chem. Commun.* **2002**, 17, 1906-1907

[11] B. Solsona, M.I. Vázquez, F. Ivars, A. Dejoz, P. Concepción, J.M. López Nieto, *J. Catal.* **2007**, 252, 271–280.

[12] Y. Liu, Patent US6355854 B1, **2001**.

[13] E. Heracleous, A.A. Lemonidou, *J. Catal.* **2006,** 237, 162-174.

[14] E. Heracleous, A.A. Lemonidou, *J. Catal.* **2010**, 270, 67-75.

[15] F. Skoufa, E. Heracleous, A.A. Lemonidou, *J. Catal.* **2015**, 322, 118-129.

[16] B. Savova, S. Loridant, D. Filkova, J.M.M. Millet, *Appl. Catal. A Gen.* **2010**, 390, 148-157.

[17] Z. Skoufa, E. Heracleous, A.A. Lemonidou, *Catal. Today* **2012**, 192, 169-176.

[18] H. Zhu, S. Ould-Chikh, D.H. Anjum, M. Sun, G. Biausque, J.-M. Basset, V. Caps, *J. Catal.* **2012**, 285, 292-303.

[19] B. Solsona, J.M. López Nieto, P. Concepcion, A. Dejoz, F. Ivars, M.I. Vazquez, J. Catal. **2011**, 280, 28-39.

[20] J.M. López Nieto, B. Solsona, R.K. Grasselli, P. Concepcion, Top. Catal. **2014**, 57, 1248-1255.

[21] H. Zhu, D.C. Rosenfeld, M. Harb, D.H. Anjum, M.N. Hedhili, S. Ould-Chikh, J.M. Basset, ACS Catal. **2016**, 6, 2852-2866.

[22] a) H. Zhu, H. Dong, P. Laveille, Y. Saih, V. Caps, J.M. Basset, Catal. Today **2014**, 228, 58-64; b) H. Zhu, D.C. Rosenfeld, D.H. Anjum, S.S. Sangaru, Y. Saih, S. Ould-Chikh, J.M. Basset, J. Catal. **2015**, 329, 291-306

[23] E. Heracleous, A. F. Lee, K. Wilson, A. A. Lemonidou, J. Catal. **2005**, 231,159-171.

[24] a) Zh. Zhang, J. Ding, R. Chai, G. Zhao, Y. Liu, Y. Lu, *Appl. Catal. A: Gen* 550 (2018) 151-159; b) Z. Zhang, G. Zhao, R. Chai, Z. Jian, Y. Liu, Y. Lu, *Catal. Sci. Technol.* **2018**, 8, 4383-4389.

[25] Z. Skoufa, E. Heracleous, A. A. Lemonidou, *J. Catal.* **2015**, 322, 118-129.

[26] B. Solsona, P. Concepción, J. M. López Nieto, A. Dejoz, J. A. Cecilia, S. Agouram, M. D. Soriano, V. Torres, J. Jiménez-Jiménez, E. Rodríguez Castellón, *Catal. Sci. Technol.* **2016**, 6, 3419-3429.

[27] I. Popescu, E. Heracleous, Z. Skoufa, A. Lemonidou, I.-C. Marcu, *Phys. Chem. Chem. Phys. **2014**, 17, 8138-8147*.

[28] I. Popescu, Z. Skoufa, E. Heracleous, A. Lemonidou, I.-C. Marcu, *Phys. Chem. Chem. Phys.* **2015**, 16, 4962-4970.

[29] J.M. López Nieto, B. Solsona, R.K. Grasselli, P. Concepcion, *Top. Catal.* **2014**, 57, 1248-1255.

[30] a) D. Delgado, B. Solsona, A. Ykrelef, A. Rodríguez-Gómez, A. Caballero, E. Rodríguez-Aguado, E. Rodríguez-Castellón, J. M. López Nieto, *J. Phys. Chem. C* **2017**, 121, 25132-25142; b) D. Delgado, R. Sanchís, J.A. Cecilia, E. Rodríguez-Castellón, A. Caballero, B. Solsona, J.M. López Nieto, *Catal. Today* **2019**, 33, 10-16.

[31] D. Delgado, B. Solsona, R. Sanchis, E. Rodríguez-Castellón, J.M. López Nieto, *Catal. Today* **2020**, in press; https://doi.org/10.1016/j.cattod.2019.06.063.

[32] E.I. Ko, J.G. Weissman, *Catal. Today* **1990**, 8, 27-36.

[33] J. Tauc, *Mater. Res. Bull.* **1968**, 3, 37-46.

[34] B.D. Viezbicke, S. Patel, B.E. Davis, D.P. Birnie III, *Phys. Status Solidi B* **2015**, 252, 1700–1710.

[35] S. Sathasivam, B.A.D. Williamson, S.A. Althabaiti, A.Y. Obaid, S.N. Basahel, M. Mokhtar, D.O. Scanlon, C.J. Carmalt, I.P. Parkin, *ACS Appl. Mater. Interfaces* **2017**, 9, 18031-18038.

[36] J.N. Kondo, Y. Hiyoshi, R. Osuga, A. Ishikawa, Y.-H. Wang, T. Yokoi, *Micropor. Mesopor. Mat.* **2018**, 262, 191-198.

[37] H.T. Kreissl, M.M.J. Li, Y.-K. Peng, K. Nakagawa, T.J.N. Hooper, J.V. Hanna, A. Shepherd, T.-S. Wu, Y.-L. Soo, S.C.E. Tsang, *J. Am. Chem. Soc.* **2017**, 139, 12670-12680.

[38] M. Grundner, J. Halbritter, *J. Appl. Phys.* **1980**, 51, 397-405.

[39] B. Solsona, J.M. López Nieto, S. Agouram, M.D. Soriano, A. Dejoz, M.I. Vázquez, P. Concepción, *Top. Catal.* **2016**, 59, 1564-1572.

[40] J. Zhang, M. Li, Z. Feng, J. Chen, C. Li, *J. Phys. Chem. B* **2006**, 110, 927-935.

[41] C. Li, M. Li, *J. Raman Spectrosc.* **2002**, 33, 301-308.

[42] N. Mironova-Ulmane, A. Kuzmin, I. Steins, J. Grabis, I. Sildos, M. Pärs, *J. Phys. Conf. Ser.* **2007**, 93, 012039.

[43] R.E. Dietz, W.F. Brinkman, A.E. Meixner, H.J. Guggenheim, *AIP Conf. Proc.* **1972**, 5, 338-338.

[44] V. Biju, M. Abdul Khadar, *J. Nanopart. Res.* **2002**, 4, 247-253.

[45] V. Biju, *Mater. Res. Bull.* **2007**, 42, 791-796.

[46] J.C. Vedrine, G. Hollinger, D. Tran Minh, *J. Phys. Chem.* **1978**, 82, 1515-1520.

[47] P. Salagre, J.L.G. Fierro, F. Medina, J.E. Sueiras, *J. Mol. Catal. A Chem.* **1996**, 106, 125-134.

[48] M.A. van Veenendaal, G.A. Sawatzky, *Phys. Rev. Lett.* **1993**, 70, 2459-2462.

[49] T. Blasco, J.M. López Nieto, *Appl. Catal. A Gen.* **1997**, 157, 117-142.

[50] E. Rojas, J.J. Delgado, M.O. Guerrero-Pérez, M.A. Bañares, *Catal. Sci. Technol.* **2013**, 3, 3173-3182.

[51] Z. Skoufa, E. Heracleous, A.A. Lemonidou, *Chem. Eng. Sci.* **2012**, 84, 48-56.

Table 1. Characteristics of support.

Sample	**Characteristics of support**	**Egap (eV)**
Support A	Nb-free PCH	-
Support B	PCH with 5wt% of Nb_2O_5	4.3
Support C	PCH with 15wt% of Nb_2O_5	4.5
Support D	PCH with 30wt% of Nb_2O_5	4.4
Nb_2O_5	Hydrothermally synthesized Nb_2O_5	3.5

Table 2. Characteristics of catalysts.

Sample	NiO wt.%	Nb_2O_5 in the support	S_{BET} (m^2/g)	NiO Crystallite size (nm) [a]	H_2-uptake [b]	LO(1P) / 2LO(2P)[c]	Egap (eV) [d]
50NiO/A	50	0	244	11	260	1.05	3.7
50NiO/B	50	5	246	9.6	228	1.47	4.0
50NiO/C	50	15	263	5.8	231	1.67	4.0
50NiO/D	50	30	165	26.1	269	0.43	3.7
20NiO/C	20	15	317	4.5	99	n.d	n.d
80NiO/C	80	15	68	32.1	403	n.d	n.d
50NiO/Nb_2O_5	50	100	61	12.4	248	n.d	3.6
NiO	100	0	15	27	490	n.d	3.6

[a)] Mean NiO crystallite size estimated by the Scherrer equation through the XRD patterns; [b)] hydrogen consumption in the TPR experiments, in mL/g; [c)] LO(1P)/2LO(2P) bands ratio in the UV-Raman spectra; [d)] Ban gap of pure Nb_2O_5 of 3.5 eV.

Table 3. Catalytic results in the ODH of ethane.[a]

Catalyst	Ethane conversion (%)	Selectivity to ethylene (%)	Catalytic activity [b]	Catalytic Activity per NiO loading [c]	STY rate of product formation [d]	TOF [e]
50NiO/A	4.5	38.6	330	659	119	4.56
50Ni0/B	7.5	67.1	549	1099	334	7.60
50NiO/C	12.7	87.5	930	1860	760	12.9
50NiO/D	11.7	64.1	857	1713	513	11.9
20NiO/C	4.2	75.2	305	1530	215	10.6
80NiO/C	11.1	53.9	813	1016	409	7.02
50NiO/Nb_2O_5	13.4 [e]	59.7	1961	3923	1094	27.2
NiO	7.5 [e]	33.3	1098	1098	339	7.6

a) At 450ºC and a contact time, W/F, of 4 g_{cat} h mol_{C2}^{-1}; **b)** Catalytic activity (in g_{C2H6}/kg_{cat} h); **c)** Catalytic activity per loading of NiO (in g_{C2H6}/kg_{NiO} h); **d)** Space time yield, STY, is the formation rate of ethylene (in g_{C2H4}/kg_{cat} h); **e)** TOF (in 10^{-4} molecules $_{C2H6}$ at^{-1}_{Ni} s^{-1}) at 450ºC and a contact time, W/F, of 2 g_{cat} h mol_{C2}^{-1}.

Caption to figures

Figure 1. Diffuse reflectance UV-VIS spectra and their corresponding Tauc plots of supports. a) Support A (PCH); b) Support B (5 wt.% Nb_2O_5 on PCH; c) Support C (15 wt.% Nb_2O_5 on PCH); d) Support D (30 wt.% Nb_2O_5 on PCH); e) Nb_2O_5.

Figure 2. Nb 3d core-level XPS spectra of Nb-containing supports, i.e. supports B, C and D. For comparison the spectrum of pure Nb2O5 has been also included.

Figure 3. XRD patterns of supported NiO catalysts. Characteristics of catalysts in Table 1. For comparison the XRD patterns of pure NiO and support C has been also included.

Figure 4. TEM images and their corresponding EDX maps of supported NiO catalysts with 50 wt% of NiO: 50NiO/A; 50NiO/B; 50 NiO/C; and 50NiO/D.

Figure 5. UV-Raman spectra of supported NiO catalysts with 50 wt% of NiO: 50NiO/A; 50NiO/B; 50 NiO/C; and 50NiO/D.

Figure 6. TPR-H_2 profiles of: a) Supported NiO catalysts, using Support C (i.e. with 15 wt.% Nb_2O_5 on PCH); b) supported NiO catalysts with 50 wt% of NiO.

Figure 7. Ni 2*p* core-level spectra of supported NiO catalysts with 50 wt% of NiO: a) 50NiO/A; b) 50NiO/B; c) 50 NiO/C; and d) 50NiO/D.

Figure 8. Nb 3*d* core-level spectra of Nb-containing supported NiO catalysts with 50 wt% of NiO: a) 50NiO/B; b) 50 NiO/C; and c) 50NiO/D.

Figure 9. Influence of NiO loading (for catalysts of xNiO/C series) (**a**) and influence of Nb-loading (for catalysts with 50wt% of NiO) (**b**) on catalytic activity (in g_{C2H6} kg_{cat}^{-1} h^{-1}) during the ODH of ethane on supported NiO catalysts. Reaction conditions: $C_2/O_2/He$ = 3/1/26 molar ratio, T = 450ºC and W/F = 4 g_{cat} h mol_{C2}^{-1}.

Figure 10. a) Variation of the selectivity to ethylene as a function of NiO-loading on Support C (15 wt.% Nb_2O_5 on PCH. b) Variation of the selectivity to ethylene (at 10% ethane conversion) as a function of ethane conversion for supported 50 wt.% NiO catalysts. Reaction conditions as in Fig. 9.

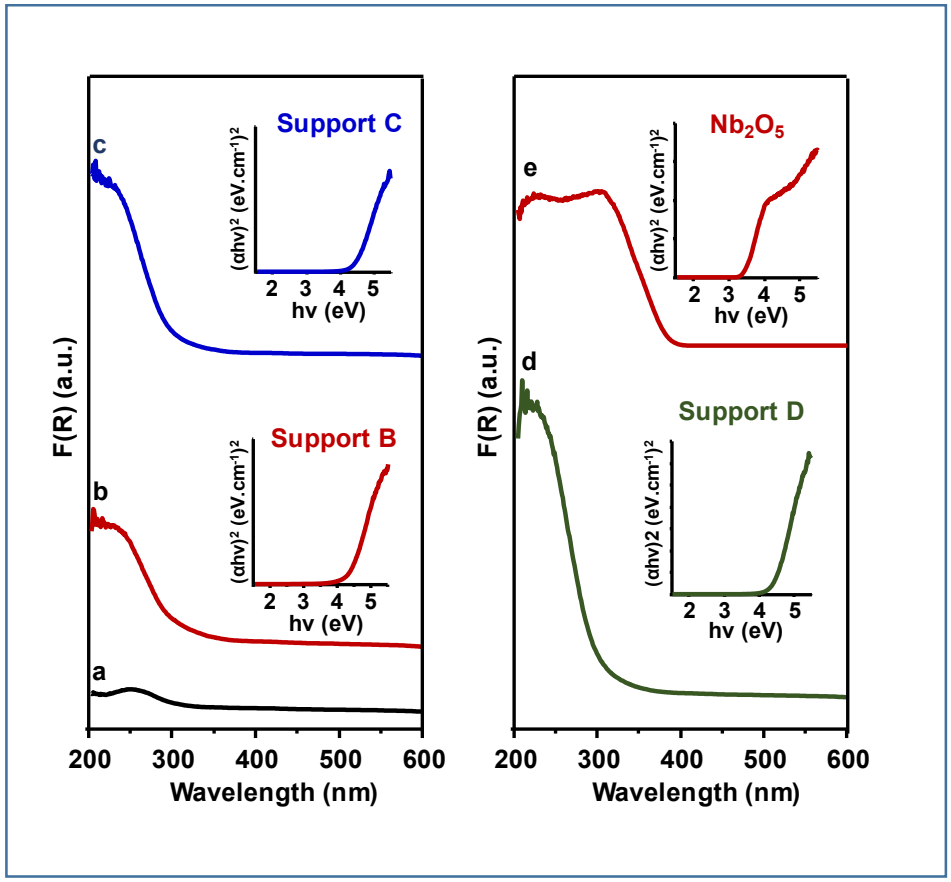
Support C
c
(αhν)² (eV.cm⁻¹)²
2 3 4 5
hv (eV)
Support B
b
a
F(R) (a.u.)
200 300 400 500 600
Wavelength (nm)
Nb2O5
e
d
Support D

Fig. 1

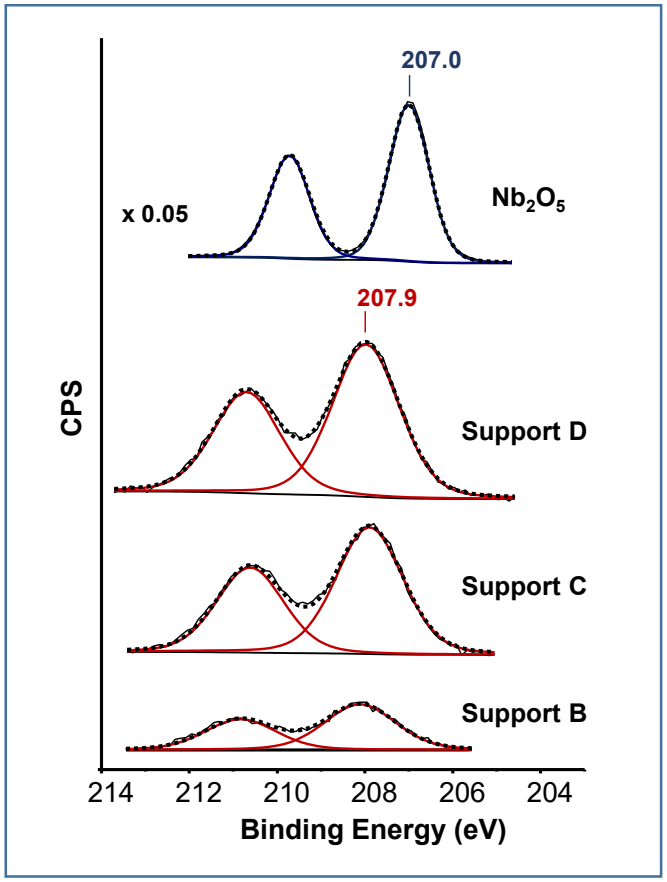
207.0
x 0.05
Nb2O5
207.9
Support D
Support C
Support B
CPS
214 212 210 208 206 204
Binding Energy (eV)

Fig. 2

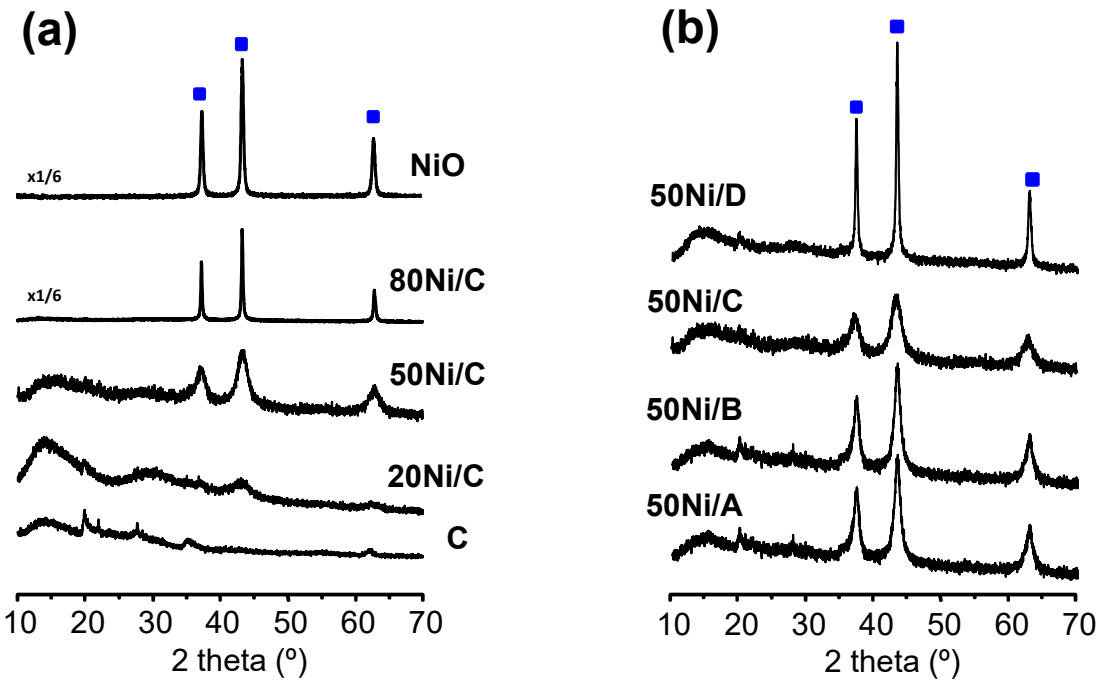
(a)
x1/6
NiO
x1/6
80Ni/C
50Ni/C
20Ni/C
C
10 20 30 40 50 60 70
2 theta (º)
(b)
50Ni/D
50Ni/C
50Ni/B
50Ni/A
10 20 30 40 50 60 70
2 theta (º)

Fig. 3

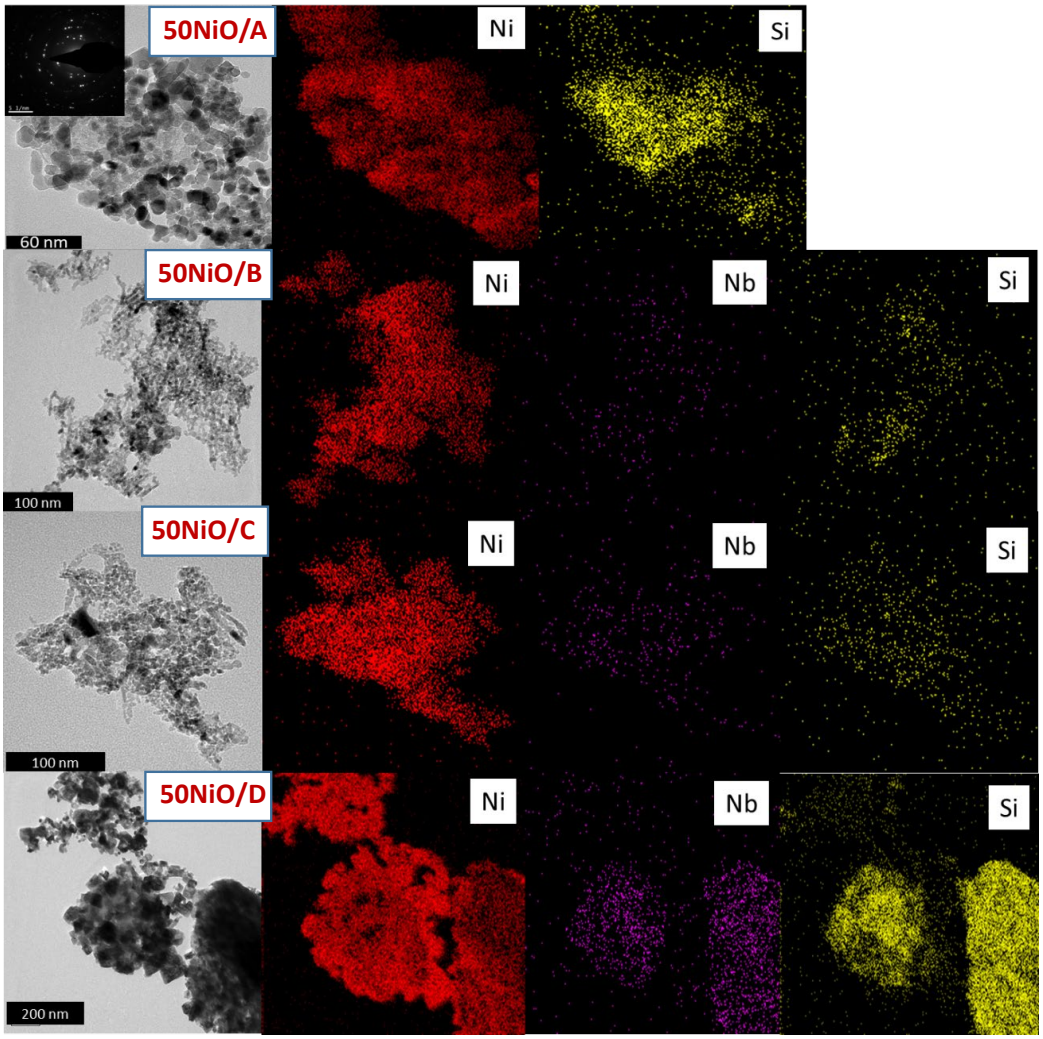
50NiO/A
Ni
Si
60 nm
50NiO/B
Ni
Nb
Si
100 nm
50NiO/C
Ni
Nb
Si
100 nm
50NiO/D
Ni
Nb
Si
200 nm

Fig. 4

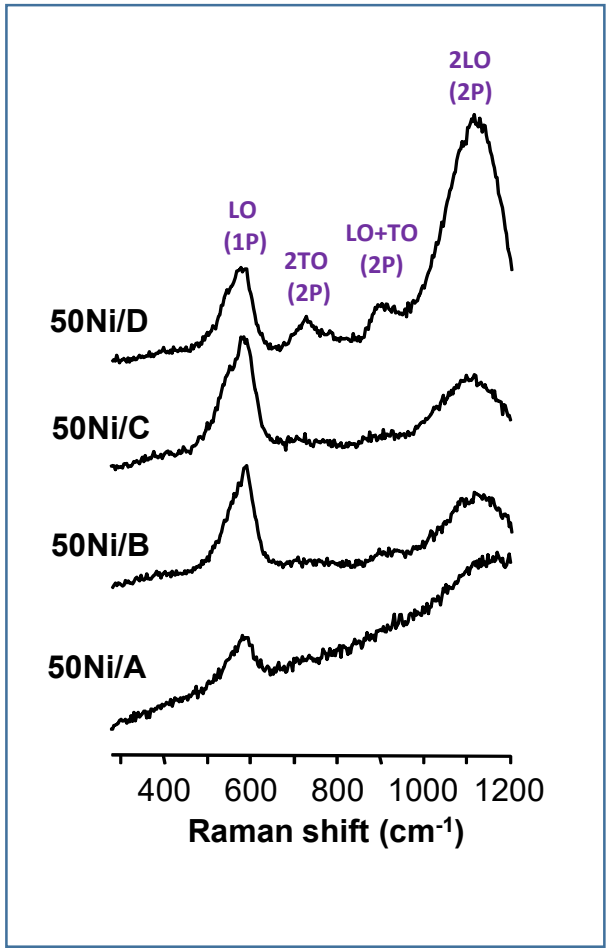
2LO
(2P)
LO
(1P)
2TO
(2P)
LO+TO
(2P)
50Ni/D
50Ni/C
50Ni/B
50Ni/A
400
600
800
1000
1200
Raman shift (cm-1)

Fig. 5

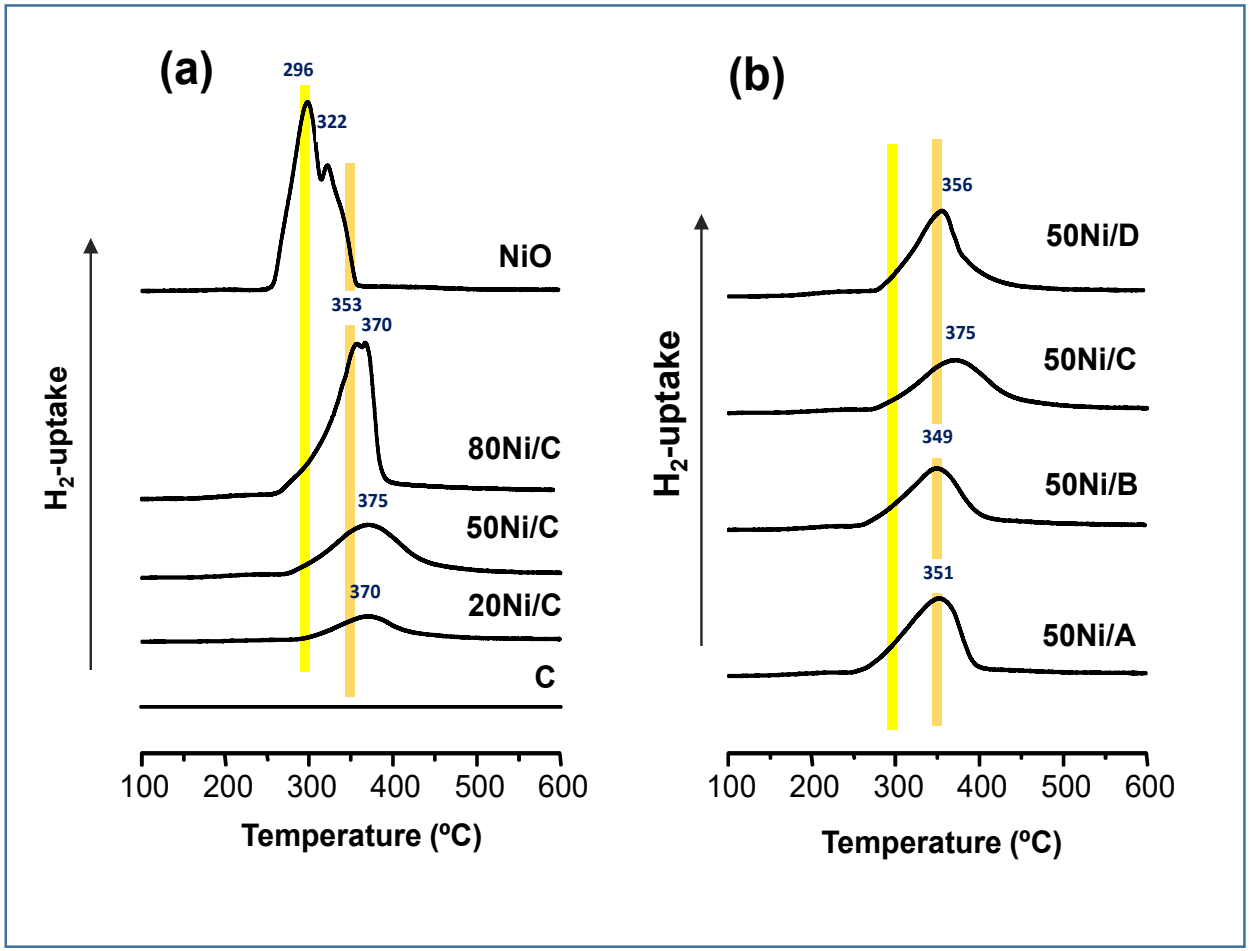
(a)
296
322
NiO
353
370
80Ni/C
375
50Ni/C
370
20Ni/C
C
H2-uptake
100
200
300
400
500
600
Temperature (ºC)
(b)
356
50Ni/D
375
50Ni/C
349
50Ni/B
351
50Ni/A
H2-uptake
100
200
300
400
500
600
Temperature (ºC)

Fig. 6

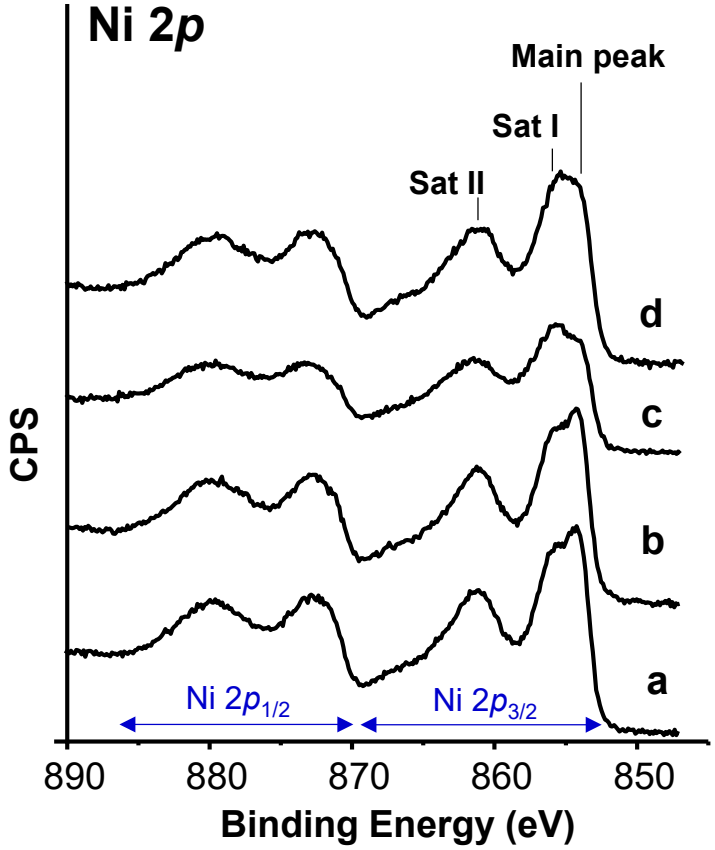
Ni 2p
Main peak
Sat I
Sat II
d
c
b
a
CPS
Ni 2p1/2
Ni 2p3/2
890
880
870
860
850
Binding Energy (eV)

Fig. 7

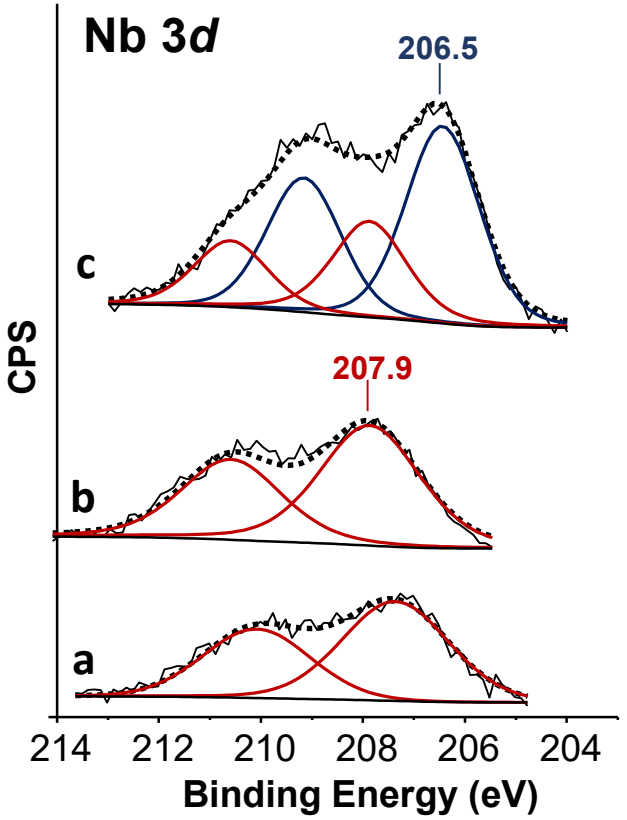
Nb 3d
206.5
c
207.9
b
a
CPS
214
212
210
208
206
204
Binding Energy (eV)

Fig. 8

Fig. 9

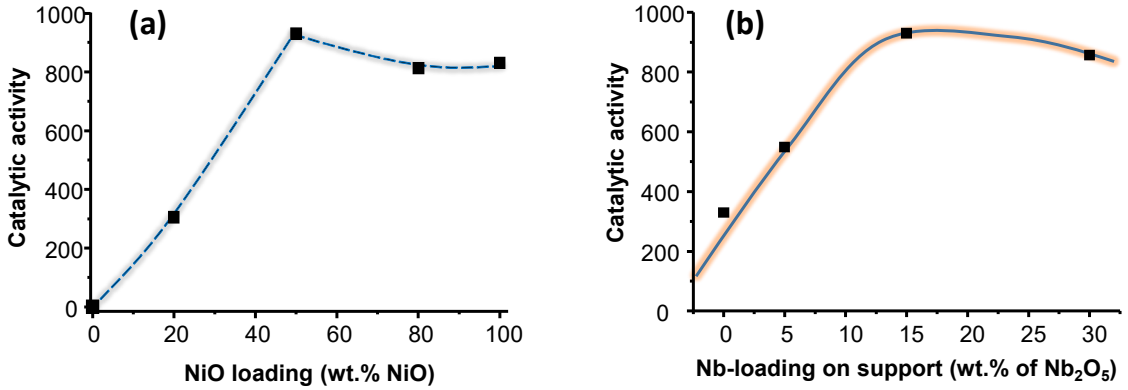
(a)
Catalytic activity
NiO loading (wt.% NiO)
(b)
Catalytic activity
Nb-loading on support (wt.% of Nb_2O_5)

Fig. 10

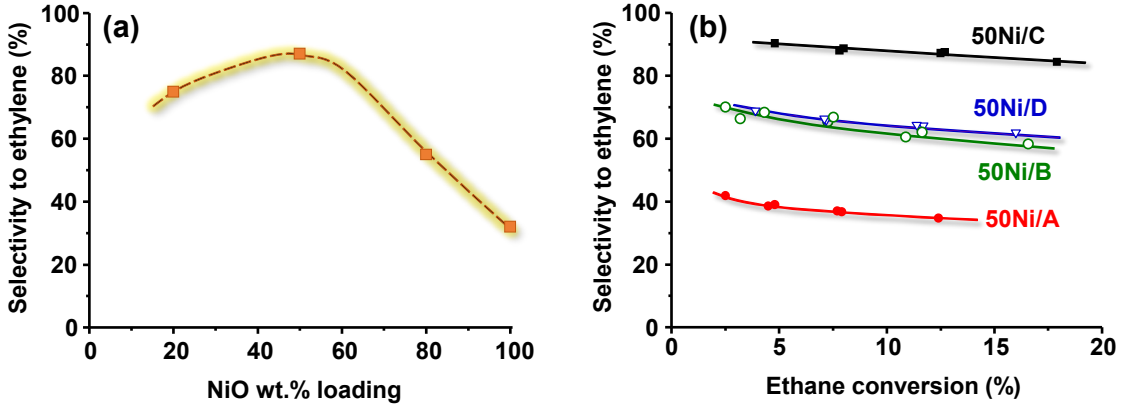
(a)
Selectivity to ethylene (%)
NiO wt.% loading
(b)
50Ni/C
50Ni/D
50Ni/B
50Ni/A
Selectivity to ethylene (%)
Ethane conversion (%)

Table of Contents

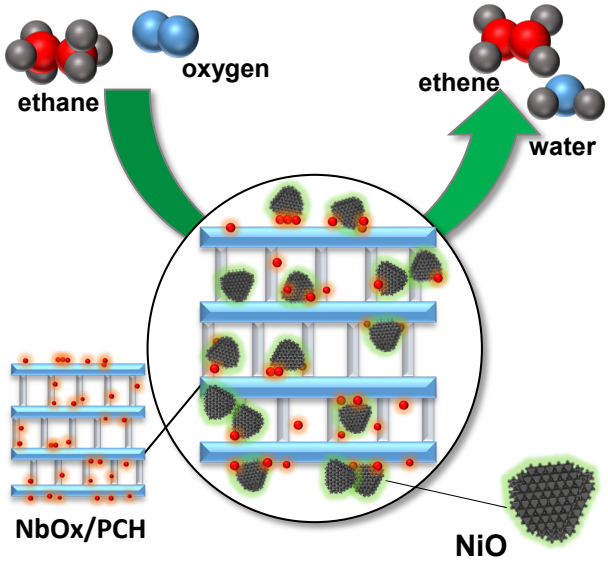

NiO supported on a Nb-containing porous clay heterostructure (PCH) shows outstanding catalytic properties in the ODH of ethane (ca. 90% selectivity to ethylene). Controlling the chemical nature of Nb^{5+} species on PCH is the key factor to achieve an effective NiO-support interaction.